Electron pair emission from surfaces: Diffraction effects

Z. Wei, F. O. Schumann,* R. S. Dhaka, and J. Kirschner
Max-Planck-Institut für Mikrostrukturphysik, Weinberg 2, D-06120 Halle, Germany
(Received 3 November 2011; revised manuscript received 19 March 2012; published 10 May 2012)

We have systematically studied the electron pair emission from a Cu(100) surface over a wide range of primary electron energies. We are able to identify contributions from valence states of different orbital characters. The relative intensity from states near the Fermi level (E_F) and from the 3*d* levels is strongly affected by the primary energy. The primary energy dependence of the pair intensity resembles the behavior of the specularly reflected primary electron beam. We discuss these findings within a kinematical diffraction model. The azimuthal orientation of the sample has a strong effect on the coincidence energy spectra. We performed measurements along two high-symmetry directions and the difference of the energy spectra reveals intensity variations up to 50%. This is an immediate consequence of the symmetry of the surface. This, in turn, proves that the depletion zone in the pair emission is nonspherical.

DOI: 10.1103/PhysRevB.85.195120 PACS number(s): 79.60.−i, 73.20.At

I. INTRODUCTION

Electrons are an essential ingredient of matter. They are responsible for the formation of chemical bonds, which lead to the emergence of crystals, for example. The material properties of these solids are decisively determined by the electronic properties. One example of the intimate relation between electrons and structure are the so-called Hume-Rothery rules for alloys containing noble metals and *sp*-valent metals.[1,2] In these alloys, the average number of valence electrons, given by n, can be controlled by the concentration. The actual value of n will determine the most stable structure. For example, if n is in the range 1–1.38, an fcc lattice is adopted. Properties like lattice constant, cohesive energy, and bulk modulus are important parameters of a solid. For transition metals, a model of constant electronic density of states of the *d* band (also termed Friedel model) is capable to reproduce the observed variation of these parameters on the *d*-band occupancy.[2,3] These two examples serve to illustrate that knowledge of the electron properties is vital for the understanding of material properties. A widely used tool in this respect is photoemission, which provides access to the electronic band structure within an effective single-electron (quasiparticle) picture.[4,5]

In contrast to atoms or molecules, solids display a variety of many-body effects, we may cite ferromagnetism as an example. The origin of this effect can be traced back to an intimate interplay of Coulomb interaction among the electrons and the Pauli principle, which leads to the exchange interaction. This complex scenario can be cast into an effective single-electron picture using a spin-split band structure. In this model, the bands of the spin-up and spin-down electrons are energetically shifted with respect to each other. This exchange-splitting has been experimentally observed by spin-resolved photoemission.[5–7] Despite the success of the quasiparticle picture, it is well known that deviations are observed in photoemission.[8–15] These are termed "many-body effects" and have its origin in the electron-electron interaction. It is obvious that a deeper understanding of the mutual electron interaction can be gained by measuring electron pairs rather than single electrons. This is possible by detecting two electrons in coincidence upon primary electron or photon excitation. This technique has matured over the years and is used for the investigations of atoms, molecules, and solid surfaces.[16–18]

As far as the presentation of coincidence data are concerned, two approaches are conceivable. First, one plots the intensity as a function of the emission angles for given kinetic energies of the outgoing electrons. Alternatively, one studies the energy spectra for given emission angles. The first approach leads to the possibility to access the exchange-correlation hole, which is a region of reduced charge density around each electron.[19–21] This important concept of solid state theory reveals itself by the emergence of a depletion zone in pair emission spectroscopy.[22–28] The second approach focusses on the valence band structure, which we investigate in this study.

The current theoretical description of the (e,2e) process on surfaces assumes that the valence band structure of the sample is satisfactorily described by a quasiparticle band structure while the interaction between electrons is described by a screened Coulomb interaction.[26,29–31] An immediate consequence is that the coincidence intensity can only occur for those energies where these valence bands have available states. We have recently verified the correctness of this assumption at least for a Cu(111) surface.[32] The general structure of the theory is such that the initial state is given by the incoming primary electron (LEED state), while the valence electron is described by a Bloch state. The two outgoing electrons are time-reversed LEED states. This formulation already emphasizes the importance of diffraction in the (e,2e) process. Diffraction is intimately related to the periodicity of scattering centers and diffraction patterns reveal the symmetry of the system. From general symmetry arguments, it is expected that the coincidence intensity depends on the azimuthal orientation of the sample. In particular, the depletion zone in angular or momentum distributions of the coincidence intensity displays the symmetry of the surface.[24,31,33]

We report on a study of a Cu(100) surface and we are able to identify the contributions from different valence states. Furthermore, we find that the energy spectra are strongly dependent on the primary energy. The relative contributions of the intensity resemble closely the LEED *I-V* curve of the (0,0) beam from a Cu(100) surface. This points clearly toward the relevance of diffraction effects, and we discuss this fact within a kinematical model extended to include diffraction of pairs. The energy spectra are affected by the azimuthal

orientation of the sample, and we find intensity variations up to 50%. These variations are a consequence of the symmetry of the depletion zone, which has the symmetry of the surface. This, in turn, proves that the depletion zone is nonspherical, which also holds for the exchange-correlation hole in real space.[34]

II. EXPERIMENTAL DETAILS

The experiments were performed in an UHV envirommment. The effect of the earth magnetic field has been reduced by using external Helmholtz coils and a mu-metal chamber. A sketch of the overall layout of the experiment is shown in Fig. 1, which has been described in more detail elsewhere.[32,35,36] It consists of two hemispherical electron energy analyzers with a mean radius of 200 mm equipped with wide angle transfer lenses and position sensitive detectors.[37] We use channel plate detectors with resistive anodes. We label the spectrometers as "left" and "right," respectively. The two electron-optical axes of the spectrometer include an angle of 90° and define the reaction plane in which the primary electrons e_0 and the detectable outgoing electrons e_{left} and e_{right} lie. The acceptance cone of the transfer lenses has an angle of 15°. Electrons have to traverse a narrow slit before entering the hemisphere. Therefore the angular acceptance is limited to a line that lies within the reaction plane. All experiments were performed with the primary beam being parallel to the normal. A Cu(100) single crystal was mounted on a standard manipulator that allows to change the azimuthal orientation of the sample. We report on studies in which either the [001] or [011] direction of the crystal is within the scattering plane. In contrast to the general operation of energy dispersive analyzers, which consists of scanning the kinetic energy of the electrons, we keep all lens voltages fixed for a given primary energy E_p. In this mode of operation, the electrons within an energy window of 10% of the pass energy are detected. All studies were performed with 100-eV pass energy, hence each spectrometer covers an energy window of 10 eV. The electron gun is equipped with a BaO anode and the energy spread of the primary beam is ∼0.3 eV.[38] The energy resolution of the coincidence experiments is 0.7 eV as judged from the energy spectra. We employ a four-way coincidence circuit in which the channel plate signals originating from the two spectrometers have to be within a time interval of 150 ns, while at the same time, the electronics of the resistive anodes indicate a successful impact position determination. If a valid event is registered, the arrival times (t_{left} and t_{right}) at the detector left and right with respect to the coincidence trigger can be determined. The resulting histogram of the time difference $t_{\text{left}} - t_{\text{right}}$ of the coincidence intensity will display a peak residing on a constant background.[32,35] The emergence of a peak is proof of *true* coincidences, whereas the background has its origin in *random* coincidences. The width of the histogram peak is a measure of the temporal dispersion of the instrument and, for the presented studies, it is 10 ns. The microscopic origin of *random* events is the excitation of the sample via two independent primary electrons. Strictly speaking, it is not possible to remove *random* events from the data set, but the aggregate effect can be removed as explained in the literature.[32,39,40] Throughout this work, we will present data corrected in this fashion. The Cu(100) surface was prepared following standard procedures of Ar sputtering and annealing cycles. All experiments were performed at room temperature. The base pressure during data acquisition was 4×10^{-11} mbar. All kinetic energies are quoted with respect to the vacuum level of the Cu(100) surface. The coincidence rate was in the range 1–2 counts per second, while the singles rates was approximately 5000 counts per second. The ratio of true to random coincidences was 1–2.

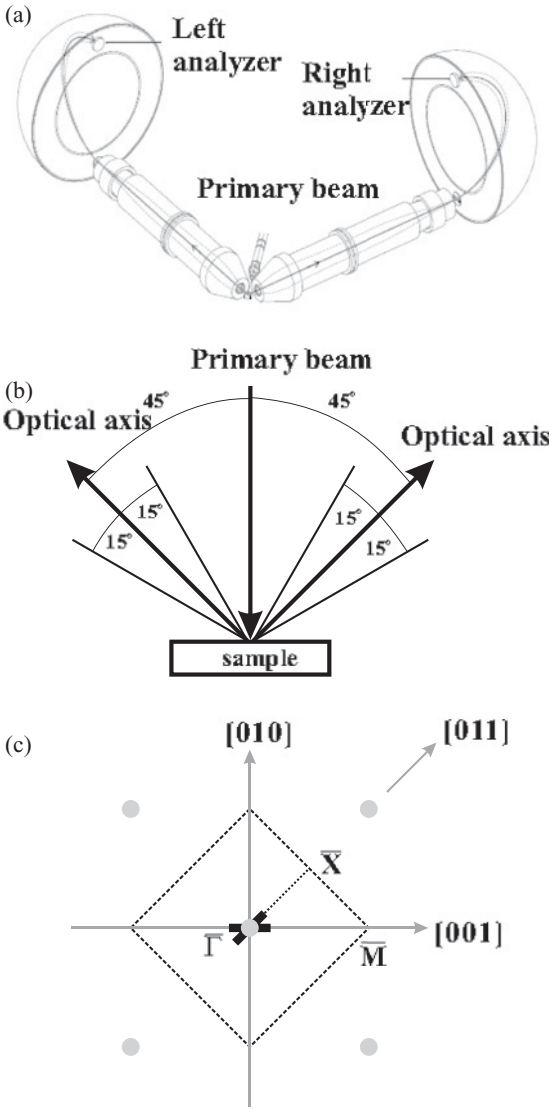

FIG. 1. (a) Sketch of the coincidence electron spectrometer. It shows two hemispherical electron energy analyzers that define a scattering plane. (b) The transfer lenses of the spectrometers are symmetrically positioned in the same plane as the primary beam. The outgoing electrons were detected at ±45° with respect to the surface normal. The angular acceptance range of ±15° with respect to mean take off angle is also shown. In (c), we indicate that the scattering plane is either along the [011] or [001] direction of the Cu(100) surface. Two black lines are centered at the $\overline{\Gamma}$ point. The length is a measure of the momentum integration within the Brillouin zone, which is ±0.4 Å^{-1}.

III. KINEMATICS AND GENERAL CONSIDERATIONS

In the (e,2e) process, an electron with well defined primary energy E_p and parallel momentum $k_{||}^p$ impacts on the surface and two electrons with kinetic energies $(E_{\text{left}}, E_{\text{right}})$ and parallel momentum $(k_{||}^{\text{left}}, k_{||}^{\text{right}})$ may be detected after overcoming the vacuum barrier given by the work function ϕ of the surface. Due to energy and momentum conservation, we obtain

$$E^p + E_{VB} = E_{\text{left}} + E_{\text{right}} + \phi = E_{\text{sum}} + \phi, \quad (1)$$

$$k_{||}^p + k_{||}^v = k_{||}^{\text{left}} + k_{||}^{\text{right}} + g = k_{||}^{\text{sum}} + g. \quad (2)$$

Here, E_{VB} and $k_{||}^v$ are the binding energy and the parallel momentum of the valence electron, respectively. These parameters can be deduced from the knowledge of the sum energy $E_{\text{sum}} = E_{\text{left}} + E_{\text{right}}$ and sum momentum $k_{||}^{\text{sum}} = k_{||}^{\text{left}} + k_{||}^{\text{right}}$ of the two outgoing electrons. The reciprocal lattice vector is labeled with g. We may read the momentum conservation as a diffraction condition. In the following, we set $g = 0$, because our low-energy studies do not allow momentum transfer. This is similar to LEED where the primary energy has to be sufficiently high to allow the observation of LEED spots. In terms of LEED nomenclature, we allow only the (0,0) beam of the pair to exist.

From Eq. (1) it follows immediately that the maximum energy an electron pair can have is given by $E_{\text{sum}}^{\max} = E^p - \phi$. Introducing the terms E_{sum} and $k_{||}^{\text{sum}}$ also emphasizes that the emitted electron pair is one entity with defined energy and momentum.

In our geometry, we probe a region of the surface Brillouin zone that is centered around the $\overline{\Gamma}$ point. The entrance lens of each spectrometer is of cylindrical symmetry and will accept electrons within a cone of an opening angle of 15°. However, a 2D-momentum sampling is not possible, because the electrons have to traverse a narrow slit before entering the hemisphere. Therefore each spectrometer can only cover a 1D-momentum range. This direction lies (for both spectrometers) in the plane defined by the electron-optical axes of the two entrance lenses. The width of this region is determined by the angular acceptance and the energy window the spectrometers cover. Typical values are ± 0.4 Å^{-1} as indicated by the length of the thick solid lines of Fig. 1(c).

In preparation of the discussion of the experimental data, it is useful to recall the basics of the electronic band structure of Cu and the Cu(100) surface, in particular. Two main contributions can be identified: a strongly dispersing sp band, which in the occupied region extends from the Fermi level E_F to 9 eV below E_F, and d states localized in an energy window 2–5 eV below E_F. The Cu(100) surface is also known to exhibit a surface state at the zone boundary in the vicinity of E_F.[41] Within our experiments we can kinematically exclude this state. On the basis of layer-resolved quasiparticle calculations,[42] we are able to present the calculated binding energy spectrum of the occupied valence states, see Fig. 2. In the following, we adopt the notion that the binding energy E_{VB} has positive values in order to maintain consistency with a recent publication.[32]

For this, we have integrated the theoretical data over the experimental momentum window centered at the Brillouin

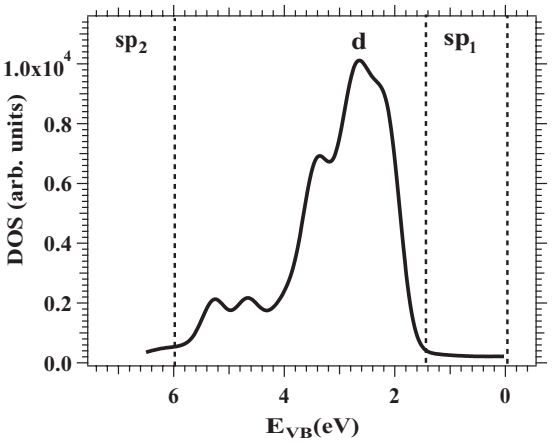

FIG. 2. The calculated quasiparticle density of states (DOS) for the Cu(100) surface is shown integrated over the angular acceptance and convoluted with a 0.5-eV wide Gaussian. The momentum integration corresponds to the black line of Fig. 1(c) and is performed if the [001] direction is in the scattering plane. For future reference, we label spectral regions with sp_1, d, and sp_2.

center, see Fig. 1(c). In order to aid comparison with experimental spectra, we convoluted with a Gaussian of 0.5 eV width representing the experimental resolution. The (e,2e) experiments are very surface sensitive and we averaged the layer resolved DOS by taking into account appropriate weighting factors. The mean-free path of the electrons detected is in the range of 3 monolayers (ML).[43–46] We consider the attenuation of the primary beam and the two outgoing electrons and the emission angle. We find that the first and second layer contribute 50% and 30% of the intensity, respectively. The remaining 20% stem from the third and deeper layers. The electronic properties of the third layer are almost identical to bulk layers. Hence we take the layer-resolved band structure of the first, second, and bulk layers and use the weighting factors 0.5 for the first, 0.3 for the second, and 0.2 for the remaining layers.

The result is shown in Fig. 2, if the [001] direction is in the scattering plane. If the [011] direction is in the scattering plane, we obtain an almost identical spectrum. The differences will be discussed in the context of azimuthal-dependent spectra to be shown below. We identify in Fig. 2 three spectral ranges that we label as sp_1, d, and sp_2. Clearly, the d-band contribution exceeds those of the sp electrons, which is easily understood if we recall the global occupation. There are ten d electrons compared to one sp electron for each Cu atom in the valence band. The broad peak in the DOS spectrum is centered at 3 eV. We emphasize that a E_{sum} spectrum is not a simple replica of the DOS spectrum. A full understanding of a coincidence spectrum requires a dedicated theoretical calculation where the single-electron band structure is an important input.[26,29–31,47] This assumption of theory has been recently confirmed by an experimental study of a Cu(111) surface.[32]

IV. PRIMARY ENERGY DEPENDENCE OF THE COINCIDENCE SPECTRUM

We performed (e,2e) experiments on a Cu(100) surface for primary electron energies E_p in the range of 20–97 eV. In Fig. 3, we display representative 2D-energy distributions for

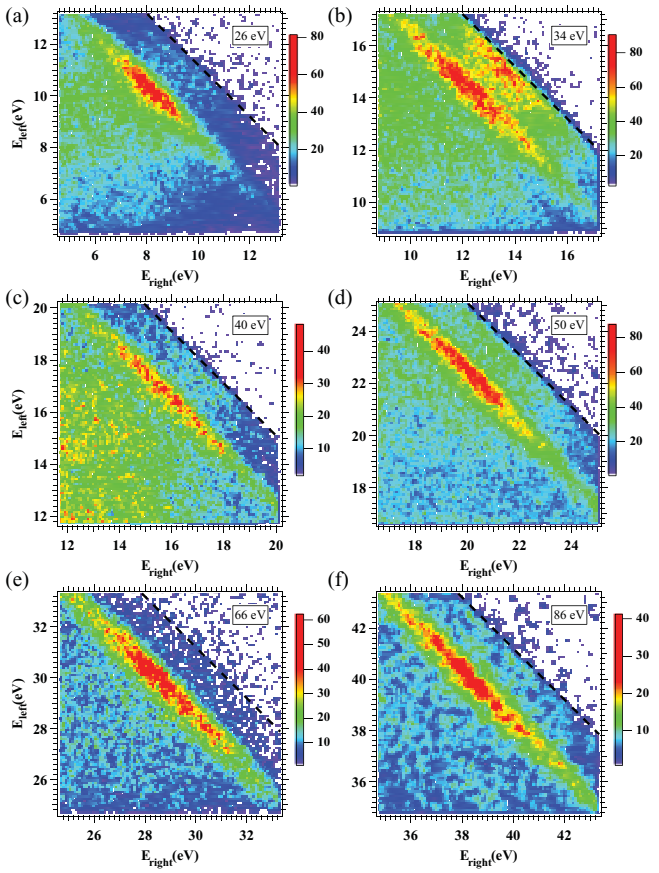

FIG. 3. (Color) 2D-energy spectra for different values of E_p. The primary energy increases from the left to the right and from the top to the bottom panel. The dashed diagonal line marks the position of $E_{\rm sum}^{\rm max}$. For these experiments, the [001] direction of the Cu(100) sample was in the scattering plane. We can clearly see high-intensity regions, which are parallel to the $E_{\rm sum}^{\rm max}$ line. Each panel on the left has a counterpart on the right. The intensity ratio between the d-band intensity and the sp_1 region is higher on the left panel compared to right side.

six different primary energies. In each of these plots, we have added a dashed diagonal line that marks the position of the maximum sum energy $E_{\rm sum}^{\rm max}$. Although we employ a symmetric geometry, the 2D-energy spectra are not fully symmetric. This is a reflection of the difficulty to mechanically align the two transfer lenses.

We can observe that the pair emission has its onset at the $E_{\rm sum}^{\rm max}$ line, which means that valence electrons from the Fermi level make a contribution. Furthermore, we see that regions of high intensity exists, which are parallel to the $E_{\rm sum}^{\rm max}$ line. This is the manifestation that valence states with fixed binding energy are involved in the emission process, see Eq. (4). Upon closer inspection, we can identify two diagonal regions. One is close to the Fermi level and is particular strong at a primary energy of 34 eV. The other region is around 3 eV below the $E_{\rm sum}^{\rm max}$ line, which usually dominates the spectrum. These intensity bands are due to the emission from d and sp_1 states, see Fig. 2.

The 2D-energy distributions have been aligned in Fig. 3 in such a way that the primary energy increases from the left to the right, likewise, E_p increases from top to the bottom. Let us focus on the intensity from the d states compared to the

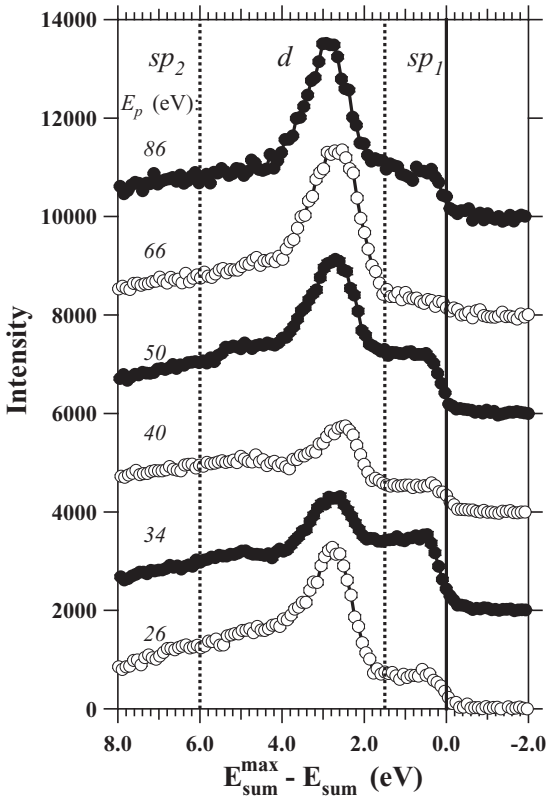

FIG. 4. The $E_{\rm sum}$ spectra for E_p in the range 26–86 eV are shown. The spectral ranges have been labeled according to the notation presented in Fig. 2. The curves with the open symbols were determined from the left panels of 2D-energy distributions in Fig. 3. Consequently, the solid symbols refer to the panels on the right side of Fig. 3. The [001] direction lies in the scattering plane.

sp_1 states. In all cases, we can see that for the left panels the ratio of d-band emission to sp_1 emission is higher than for the right panels. This means that the relative intensities display a nonmonotonic behavior as a function of E_p.

This fact can be accentuated by computing $E_{\rm sum}$ distributions from the 2D-energy presentations. For this, we determine for each coincidence event the value of $E_{\rm sum}$. If we were to set $E_{\rm left} = E_{\rm right}$, we would consider a symmetric scenario that also has been adopted in the theoretical (e,2e) calculations.[31,33,47] However, in order to have sufficient statistics for the plots, we do not impose a further constraint. Comparing $E_{\rm sum}$ spectra obtained for different excitation energies is facilitated by plotting the intensity as a function of $E_{\rm sum}^{\rm max} - E_{\rm sum}$. Emission of pairs, which involve states at the Fermi level, occurs at $E_{\rm sum}^{\rm max} - E_{\rm sum} = 0$. This procedure is the equivalent of setting the binding energy zero at E_F in photoemission. In Fig. 4, we present an overview of different $E_{\rm sum}$ spectra from the 2D-energy distributions shown in Fig. 3. The curves with the open symbols were determined from the left panels of 2D-energy distributions in Fig. 3. Consequently, the solid lines refer to the panels on the right side of Fig. 3. In all cases, we can observe that the pair emission starts at $E_{\rm sum}^{\rm max} - E_{\rm sum} = 0$ as commented above, we have marked this energy position by a solid vertical line. From the onset, we can also determine the energy resolution of the coincidence experiment, which we quote as 0.8 eV. On the basis of the

calculated DOS spectrum displayed in Fig. 2, we divide the coincidence spectra into three parts that we label in analogy with sp_1, d, and sp_2. The following facts emerge from this presentation. The peak of the d-band contribution is centered at $E_{\rm sum}^{\rm max} - E_{\rm sum} = 3$ eV, which is in line with the DOS distribution shown in Fig. 2. Starting at $E_p = 26$ eV, the d-band contribution is about a factor of 4 larger than the sp_1 contribution. Increasing E_p to 34 eV leads to almost identical intensity contributions as can be also clearly seen with the 2D-energy plot of Fig. 3(b). Further increase of E_p to 40 eV has the consequence that the d-band intensity dominates the spectrum. At $E_p = 50$ eV, the sp_1 intensity has grown again and almost vanishes at $E_p = 66$ eV. Finally, at $E_p = 86$ eV, the sp_1 region has increased in intensity again. The nonmonotonic behavior as a function of E_p has been highlighted in Fig. 4 by plotting the $E_{\rm sum}$ spectra by either open or solid symbols. Open symbols refer to a relatively weak sp_1 contribution, while the solid symbols refer to a relatively strong sp_1 contribution. From the different $E_{\rm sum}$ spectra displayed in Fig. 4, it is apparent that the relative contributions of the spectral regions labeled as sp_1, sp_2, and d depend on the primary energy E_p. A surprising result is that the intensity in the region sp_1 can be comparable to the $3d$ region. We recall that the $3d$ band is fully occupied with ten electrons, while the sp band has an occupancy of one electron. Taking into account that the sp band has a bandwidth of 9–10 eV, it becomes apparent that the energy window within 2 eV of E_F offers more than an order of magnitude less available states. The most appropriate way is to present the coincidence intensity for constant primary flux. From this, we can directly observe the E_p dependence of the three spectral regions. However, during the course of these experiments, we were not equipped to measure the low primary flux impinging on the sample. Therefore we are not able to distinguish between an enhancement of the sp_1 region or an reduction of the $3d$-band intensity. Nevertheless, there is a mechanism that effectively enhances the sp_1 intensity. An alternative way of presenting the data is to integrate the intensity of the whole $E_{\rm sum}$ spectrum, which leads to the intensity $I(sp_1 + d + sp_2) = I(\text{total})$. Likewise, we can integrate over the sp_1 region alone and obtain the intensity $I(sp_1)$. We proceed and determine the ratio $I(sp_1)/I(\text{total})$ for each value of E_p, the resulting curve is presented in Fig. 5. It is apparent that the relative contribution of sp_1 displays a nonmonotonic dependence with maxima at $E_p = 34$, 46, and 86 eV. We have included in Fig. 5 the E_p dependence of the LEED (0,0) beam obtained with a near normal incidence beam (3° off normal).[48] The curves of the coincidence data and LEED intensity bear a strong resemblance. This clearly suggests the relevance of diffraction in the (e,2e) process. As a matter of fact, the theoretical description of the (e,2e) process incorporates a multiple scattering process.[26,29–31,47] The incoming beam is described by a LEED state, while the outgoing electrons are described as time-reversed LEED states. This means that diffraction of the primary beam and diffraction of the pair are dealt with on an equal footing. LEED and, in particular, the analysis of the LEED I-V curves are an established method to determine structural parameters of surfaces. A full interpretation requires multiple scattering calculations.[49] On the other hand, the I-V curve of the (0,0) beam can be satisfactorily discussed within a kinematical framework. A

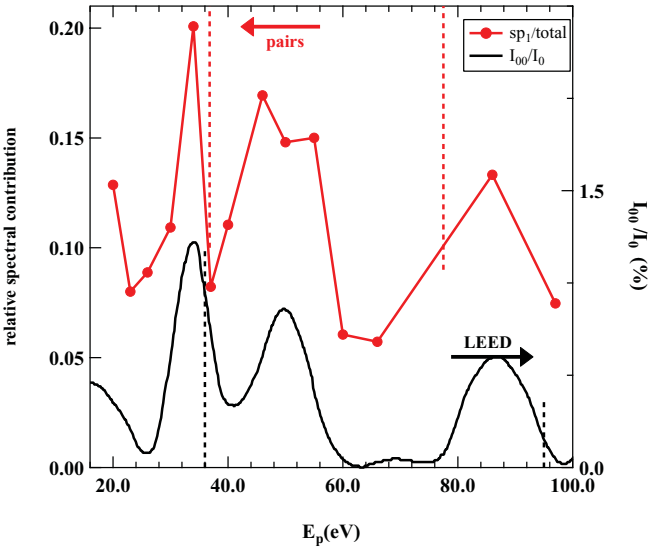

FIG. 5. (Color) The red curve shows the primary energy dependence of the normalized intensity spectral region $I(sp_1)/I(\text{total})$. For comparison, we also plot as black curve the published data of the LEED I-V curve of the (0,0) beam from a Cu(100) surface.[48] This experiment was performed with an angle of incidence of 3°. The dashed black (red) lines indicate the energy position of Bragg maxima within a kinematical model for single electron and pair diffraction as discussed in the text.

reasonable result of the layer-averaged perpendicular lattice constant can be thus obtained. The emergence of intensity maxima in the (0,0) I-V curve are due to the fulfillment of a third Laue condition along the surface normal. The close resemblance of the two curves in Fig. 5 suggest an important contribution due to diffraction in the coincidence events.

Our geometry is also referred to as a reflection experiment, because the emitted electrons have a momentum component pointing away from the surface, while the primary beam is pointed toward the sample. This means that there is a process that reverses the momentum direction. A LEED (0,0) beam is the manifestation of such a process and we may consider this beam as the "primary" beam. In such a picture, we have effectively a transmission experiment through the last few layers. Let us suppose that we perform the experiment with constant primary flux for different values of E_p. This leads to the notion that via the E_p dependence of the (0,0) beam we perform the experiment effectively with varying primary flux, see the black curve in Fig. 5. Hence we expect all three spectral regions to be modulated via the E_p dependence of the specular beam. If we calculate the intensity ratio $I(sp_1)/I(\text{total})$, we remove this dependence and what is left is a variation due to the pair emission alone. The interesting point is that this curve still resembles the one for the specular beam. For a further explanation, we explore diffraction of electron pairs.

Evidence of diffraction of pairs with momentum transfer in the surface plane has been reported before.[50,51] Hence, one may wonder whether also diffraction of pairs along the surface normal plays a role. For this, we want to discuss pair diffraction within a kinematical model that is basically an extension of the model used for the LEED (0,0) beam. We have introduced this

concept in a recent publication and provided the final result.[32] In this work, we provide a more detailed account. We point out that a similar scheme has been proposed and used in the context of photoemission.[52–54] For LEED, the primary energy E_P^{00} at normal incidence that results in a Bragg peak is given by the equation[49]

$$E_p^{00} = \frac{n^2h^2}{8md^2} - V_0, \quad n = 1,2,\ldots. \tag{3}$$

The inner potential V_0 for Cu is approximately 10 eV. The electron mass and Planck constant are given by m and h, respectively. The layer separation is determined by d. The prediction of this model is in fair agreement with the experimental observation.[55,56] The picture on which the above equation is based determines the wavelength λ inside the crystal. Similar to an optical etalon, the path difference taken by the electron is $2d$. For constructive interference to occur, the condition $2d/\cos(\theta)=n\,\lambda$ must hold. Obviously choosing $n = \frac{1}{2}, \frac{3}{2}, \ldots$ leads to destructive interference.

Along the same line, we can formulate a diffraction condition for pairs. The key point is to treat the electron pair as one quasiparticle with defined sum momentum and sum energy. If we consider, for the time being, only valence states near E_F, then the energy sum of the emitted pair is equal to $E_{\rm sum}^{\rm max} = E_p - \phi$, see Eq. (1). This is the energy in the vacuum region, but we need to determine the wavelength in the crystal. This requires the knowledge of the inner potential for a pair. The simplest approximation is to use twice the value of a single electron. This leads to the left-hand side of the following equation:

$$(E_p - \phi) + 2V_0 = \frac{\hbar^2}{2(2m)}\mathbf{k}_{\rm sum}^2. \tag{4}$$

The available energy is stored in the center-of-mass motion of a particle with mass $2m$ and total momentum vector $\mathbf{k}_{\rm sum}$. This vector has a component in the plane $k_{||}^{\rm sum}$ and perpendicular $k_{\perp}^{\rm sum}$ to it. We recall that in our geometry $k_{||}^{\rm sum} \approx 0$, hence Eq. (4) describes the behavior of $k_\perp$. We can rearrange this equation to yield

$$k_\perp = \sqrt{\frac{4m}{\hbar^2}(E_p - \phi + 2V_0)}. \tag{5}$$

The momentum along the normal direction $k_\perp$ is directly related to the wave length $\lambda_\perp$ in this direction. For the usual constructive interference condition, we finally obtain

$$n\lambda_\perp = n\frac{2\pi}{k_\perp} = 2d, \quad n = 1,2,\ldots. \tag{6}$$

What is left to do at this point is to perform straightforward rearrangements, which leads to the following expression for the primary energy to yield a diffraction condition for pairs:

$$E_p = \frac{h^2n^2}{16md^2} + \phi - 2V_0. \tag{7}$$

We note that the first term in this expression is almost half of the right-hand side of Eq. (3), which determines the primary energy E_p^{00} for which a LEED maximum is achieved. In order to have a more compact expression, we replace the first term of Eq. (7) by rearranging Eq. (3) and obtain

$$E_p = \tfrac{1}{2}E_p^{00} - \tfrac{3}{2}V_0 + E_{VB} + \phi. \tag{8}$$

Since no in-plane momentum transfer occurs, we may term this pair diffraction beam also as (0,0) in analogy to the common LEED notation. In the last step, we also allow valence states that do not reside at E_F. We recall that we use the convention that adopts positive values for E_{VB}. According to Eq. (8), constructive interference occurs if the E_p value increases by an amount given by E_{VB}.

TABLE I. Calculated Bragg peaks (E_p, eV) for the (0,0) beam from the Cu(100) surface in kinematic approximation. We set the binding energy $E_{VB} = 0$ in Eq. (8).

Order	Single electron	Electron pair
1	1.5	−9.2
2	36.2	8.1
3	94.0	37.0
4	174.9	77.5

In Table I, we compare the predicted primary energies for which Bragg maxima occur in single-electron and pair-electron diffraction. For the later, we set $E_{VB} = 0$ in Eq. (8). We notice that for rather similar energies diffraction maxima occur. The first-order peak for pairs occurs for a negative value of E_p. This means that the pair diffraction occurs within the solid and can not be observed outside the surface. We have included the kinematically derived values in Fig. 5 as dashed vertical lines. For the LEED (0,0) beam, the first predicted peak within the measured energy window occurs at 36 eV, which matches the experimental observation reasonably well. However, the second peak at 46 eV is clearly missed in the model, which is a shortcoming of the kinematical model. The third peak is predicted to be at 94 eV, while the experiment puts the peak at 85 eV. The three peaks in the normalized coincidence intensity $I(sp_1)/I(\text{total})$ are also not fully reproduced. In analogy to the LEED case, the peak around 50 eV is completely missed, while the peaks at 34 and 86 eV are reasonably well reproduced.

One of the predictions of Eq. (8) is that the E_p value for constructive interference shifts with the binding energy. As far as the sp_2 region is concerned, we can observe such a behavior, although the peaks are not as clearly visible as for the sp_1 region. The relative intensity of the d-band region does not follow the prediction of our model. Obviously, the orbital character plays a role and we note that the kinematical picture is an effective plane wave model. Hence, we can understand qualitatively the deviation for the d-band region.

The shortcomings of the kinematical picture for both the LEED and pair diffraction make it mandatory to perform dynamical calculations. As far as LEED is concerned, codes for this are available and the determination of structural parameters is an established technique. Therefore the reproduction of the LEED I-V curve as displayed by the black curve in Fig. 5 is straightforward. However, the situation for a dynamical (e,2e) calculation is more complicated. In principle, one can determine the E_p dependence for the different spectral regions. However, current theoretical (e,2e) studies are limited to a maximum E_p value in the range of 30 eV. Extending the

calculations to higher primary energies requires to include higher values of the angular momentum for the partial wave expansion. This, in turn, leads to an increase in computation time that effectively prevents a theoretical study covering the E_p range of the present experiment. Nevertheless, our model emphasizes the importance of one particular scattering path within the multiple scattering description. This may be used as input for theory to simplify the computation.

We conclude that we have provided evidence that diffraction of the emitted pair has a strong impact of the coincidence spectra. A simple kinematical picture captures some of aspects of the observations, while a full explanation requires a dynamical approach.

V. AZIMUTH-DEPENDENT COINCIDENCE SPECTRA

As discussed in the introduction, general symmetry arguments dictate that the coincidence intensity depends on the sample orientation. Our experiment has a scattering plane defined by the electron-optical axis of the lenses and we probe only the valence band momentum within this plane, see Fig. 1(c). We investigated how the E_{sum} spectra are affected if two different main symmetry directions are studied. We selected the azimuthal orientation of the sample such that the scattering plane captures either the [011] or [001] direction.

For this, we focused on the E_p range 30–40 eV. We recall from Fig. 5 that in this regime, the contribution from the sp_1 region changes rapidly and has its highest relative contribution for 34 eV.

Despite the fact that the absolute primary flux was not known, spectra obtained with the same E_p but different azimuth can be directly compared, because of the stability of the electron gun. Difference in the data acquisition time can be easily accounted for by dividing the obtained counts by the acquisition time. In this manner, we derive the intensity in counts per second rather than accumulated counts.

This procedure leads to the spectra displayed in Fig. 6. The red data points refer to the [011] orientation, while the blue data points concern the experiments along the [001] direction.

We can clearly observe that the azimuthal orientation has a strong impact on the spectra apart from the region sp_2, which stays almost constant. For all E_p values studied, the [011] orientation gives a larger coincidence intensity. In order to quantify the difference in the spectra, we computed, at the energy positions given by the arrows, the difference divided by the sum of the spectra. At $E_p = 30$ eV, the main difference is at $E_{\text{sum}}^{\text{max}} - E_{\text{sum}} = 2.7$ eV. At this energy position, the difference amounts to 20%. Increasing E_p to 34 eV changes both spectra compared to $E_p = 30$ eV by a larger relative contribution of the spectral range sp_1. However, the difference is still 17% and confined to the d region. Upon further increase of E_p to 36 eV both the d-band and sp_1 regions show an azimuthal dependence of 31% and 29%, respectively. Finally, at $E_p = 40$ eV, the azimuthal dependence becomes even stronger, which is 41% for the d region and 51% for the sp_1 region.

These experimental findings can be brought in the context of the exchange-correlation hole and its manifestation in angular or momentum distributions. For this, we display in Fig. 7(b) a theoretical momentum distribution for a Cu(100)

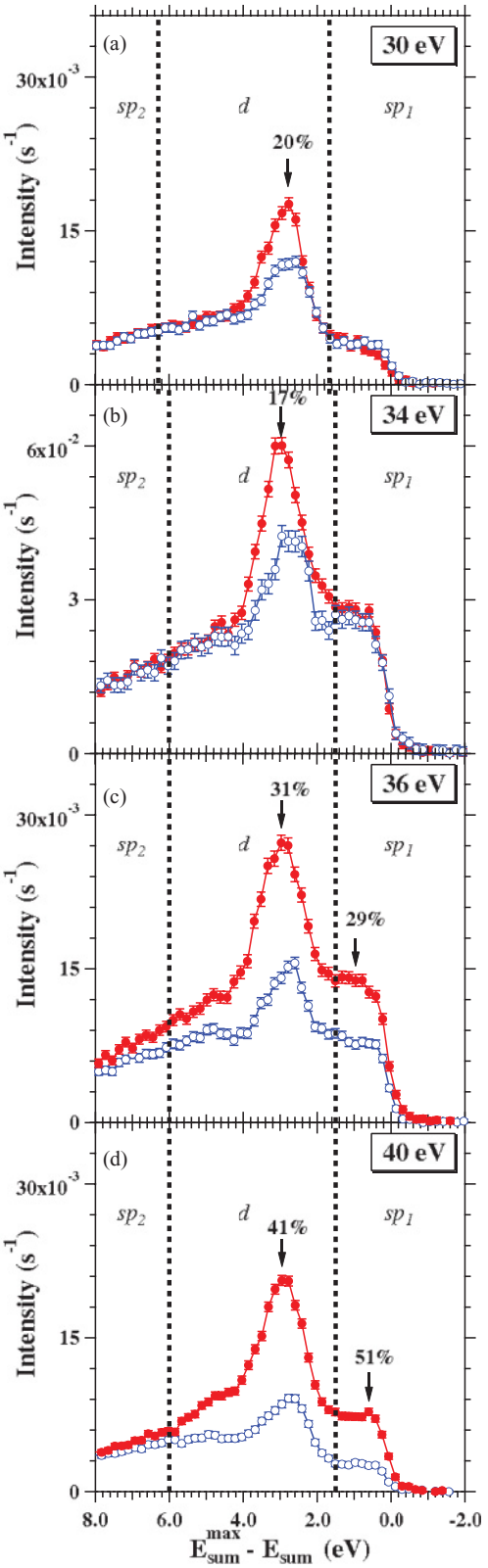

FIG. 6. (Color) The azimuthal angle (ϕ) dependent sum energy spectra of the Cu(001) surface are shown. The primary electron energies are in the range 30–40 eV. The intensities are presented in count rate (s^{-1}). The data for reaction plane along the [011] ([001]) direction are indicated by red (blue) symbols. At the energy positions marked by the arrows, we computed the ratio of the difference and the sum of the E_{sum} spectra.

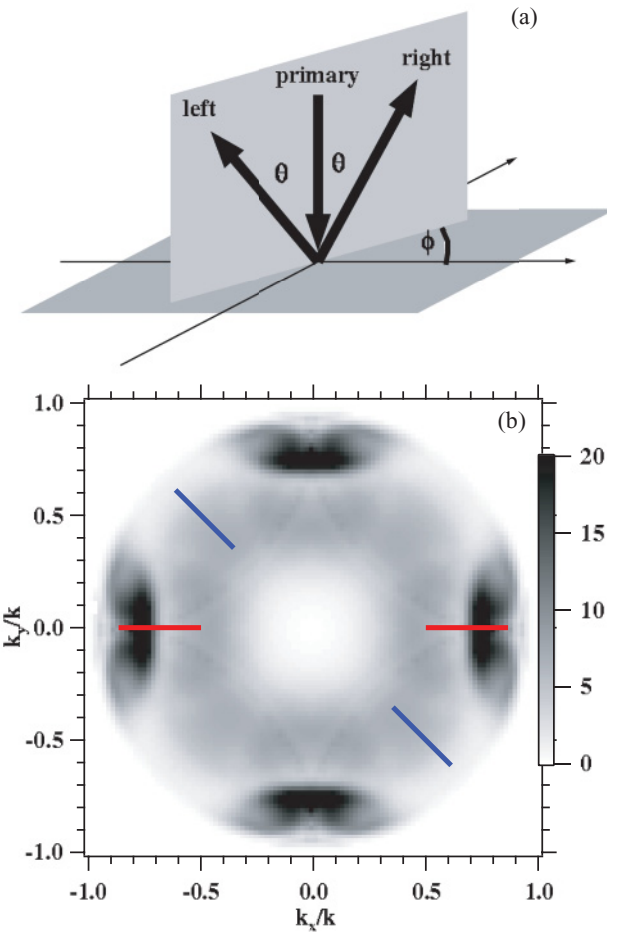

FIG. 7. (Color) (a) describes the geometry assumed by the (e,2e) calculation for the momentum distribution plotted in (b). In (b), we present the result for a Cu(100) surface excited with $E_p = 29.7$ eV.[57] The energy of the outgoing electrons ensures that the valence electron originates from the d-band region, see Fig. 2. Included in this plot are pairs of lines that indicate which part the experiment is able to cover. The red (blue) lines refer to the experiment where the scattering plane includes the [001] ([011]) direction.

surface excited with $E_p = 30$ eV. For details on how this is calculated, we refer to a recent work by Giebels *et al.* who display analogous momentum distributions for (e,2e) from a Cu(111) surface.[33] The geometry assumed by the calculation is explained by the sketch of Fig. 7(a). A surface is excited by a normal incidence primary electron beam. The emitted electrons constituting a pair have the same kinetic energy and leave the sample with the emission angle θ but in opposite directions. The pair defines a plane with has an angle ϕ with respect to a crystallographic axis, for example the [001] direction. If all possible choices of θ and ϕ are evaluated, the intensity as a function of the in-plane momentum components can be displayed. This is shown in Fig. 7(b) for the case of a Cu(100) surface excited by a primary beam with $E_p = 29.7$ eV. The energy of the two outgoing electrons is fixed to 11.6 eV, which means that $E_{\text{sum}}^{\text{max}} - E_{\text{sum}} = 2$ eV. In other words, the valence electron originates from the spectral d-band region. This choice of energies is motivated by the experimental study that showed for E_p in the range 30–40 eV the strongest azimuthal variation, see Fig. 6. It is obvious that this 2D-momentum distribution exhibits the fourfold symmetry of the surface. The very small intensity (or depletion zone) near the origin is the manifestation of the exchange-correlation hole as previously discussed in experiment and theory.[22–24,26–28,31,33] Apart from the fourfold symmetry, we note also rather strong intensity variations. In contrast to theory, our experiment captures only a fraction of the half-space as indicated by the pair of blue and red lines in the momentum distribution of Fig. 7(b). As stated above, the narrow entrance slit allows to sample only one component of the in-plane momentum of the emitted electrons.

Although we integrate over these regions, strong intensity variations are still predicted. If we compute in the same fashion as for the experimental data the ratio of the difference and the sum, we obtain a value of 30%. This agrees rather well with the experimental azimuthal variations. The calculated 2D-momentum distribution for a different $E_{\text{sum}}^{\text{max}} - E_{\text{sum}}$ value will be different from the one displayed in Fig. 7(b), but will exhibit also a fourfold symmetry. If the intensity within the lines is determined from different $E_{\text{sum}}^{\text{max}} - E_{\text{sum}}$ values, a sum energy spectrum of the kind shown in Fig. 6 will result. These are predicted to be dependent on the azimuthal direction that is clearly experimentally verified. This, in turn, means that the azimuthal dependence of the E_{sum} spectra is a direct proof that the depletion zone is anisotropic or nonspherical.

VI. SUMMARY

We have presented a systematic study of the pair emission from a Cu(100) surface. The 2D-energy distributions display diagonal intensity bands, which is clear proof that valence states with well defined binding energy are present. The energy positions of the diagonal bands can be understood by an effective single electron band structure. This supports the theoretical description that uses such a band structure as input. We also observed that the relative coincidence intensity of the sp_1 region displays a nonmonotonic behavior as a function of primary energy. The sp_1 region resembles the intensity variation of the (0,0) LEED I-V curve. This strongly supports the notion that diffraction is an important ingredient in the description of the (e,2e) process. We invoke a kinematical model for diffraction for both primary electron beam and pair intensity to explain the intensity features qualitatively. We observe a strong effect of the azimuthal orientation on the energy spectra, variations up to 50% are found. These variations are in line with a theoretical (e,2e) calculation. This variation is related to the nonspherical depletion zone in the momentum distributions of the pairs.

ACKNOWLEDGMENTS

We thank H. Gollisch and R. Feder for stimulating discussions and for providing the theoretical quasiparticle density of states of the Cu(100) surface together with the (e,2e) momentum distribution. Funding from the DFG through SFB 762 is gratefully acknowledged.

*schumann@mpi-halle.de

[1] C. Kittel, *Introduction to Solid State Physics* (Wiley, New York, Chichester, Brisbane, Toronto, Singapore, 1991).

[2] D. Pettifor, *Bonding and Structure of Molecules and Solids* (Clarendon Press, Oxford, 1995).

[3] W. A. Harrison, *Electronic Structure and the Properties of Solids* (Dover, New York, 1989).

[4] *Photoemission and the Electronic Properties of Surfaces*, edited by B. Feuerbacher, B. Fitton, and R. F. Willis (Wiley, Chichester, New York, Brisbane, Toronto, 1978).

[5] S. Hüfner, *Photoelectron Spectroscopy* (Springer, Berlin, Heidelberg, New York, Hong Kong, London, Milan, Paris, Tokyo, 2003).

[6] E. Kisker, K. Schröder, M. Campagna, and W. Gudat, Phys. Rev. Lett. **52**, 2285 (1984).

[7] *Polarized Electrons In Surface Physics*, edited by R. Feder (World Scientific, 1985).

[8] S. Monastra, F. Manghi, C. A. Rozzi, C. Arcangeli, E. Wetli, H.-J. Neff, T. Greber, and J. Osterwalder, Phys. Rev. Lett. **88**, 236402 (2002).

[9] J. Sánchez-Barriga, J. Fink, V. Boni, I. Di Marco, J. Braun, J. Minár, A. Varykhalov, O. Rader, V. Bellini, F. Manghi, H. Ebert, M. I. Katsnelson, A. I. Lichtenstein, O. Eriksson, W. Eberhardt, and H. A. Dürr, Phys. Rev. Lett. **103**, 267203 (2009).

[10] J. Sánchez-Barriga, J. Minár, J. Braun, A. Varykhalov, V. Boni, I. Di Marco, O. Rader, V. Bellini, F. Manghi, H. Ebert, M. I. Katsnelson, A. I. Lichtenstein, O. Eriksson, W. Eberhardt, H. A. Dürr, and J. Fink, Phys. Rev. B **82**, 104414 (2010).

[11] R. Clauberg, W. Gudat, E. Kisker, E. Kuhlmann, and G. M. Rothberg, Phys. Rev. Lett. **47**, 1314 (1981).

[12] G. van der Laan, M. Surman, M. A. Hoyland, C. F. J. Flipse, B. T. Thole, Y. Seino, H. Ogasawara, and A. Kotani, Phys. Rev. B **46**, 9336 (1992).

[13] F. Manghi, V. Bellini, J. Osterwalder, T. J. Kreutz, P. Aebi, and C. Arcangeli, Phys. Rev. B **59**, R10409 (1999).

[14] G. van der Laan, J. Zaanen, G. A. Sawatzky, R. Karnatak, and J.-M. Esteva, Phys. Rev. B **33**, 4253 (1986).

[15] T. Valla, A. V. Fedorov, P. D. Johnson, and S. L. Hulbert, Phys. Rev. Lett. **83**, 2085 (1999).

[16] L. Avaldi and A. Huetz, J. Phys. B **38**, S861 (2005).

[17] J. Ullrich, R. Moshammer, A. Dorn, R. Dörner, L. P. H. Schmidt, and H. Schmidt-Böcking, Rep. Prog. Phys. **66**, 1463 (2003).

[18] *Correlation Spectroscopy of Surfaces, Thin Films, and Nanostructures*, edited by J. Berakdar and J. Kirschner (Wiley-VCH, 2004).

[19] E. Wigner and F. Seitz, Phys. Rev. **43**, 804 (1933).

[20] J. C. Slater, Rev. Mod. Phys. **6**, 209 (1934).

[21] P. Fulde, *Electron Correlations in Molecules and Solids*, Springer Series in Solid-State Sciences Vol. 100 (Springer, Berlin, 1991).

[22] F. O. Schumann, J. Kirschner, and J. Berakdar, Phys. Rev. Lett. **95**, 117601 (2005).

[23] F. O. Schumann, C. Winkler, G. Kerherve, and J. Kirschner, Phys. Rev. B **73**, 041404(R) (2006).

[24] N. Fominykh, J. Berakdar, J. Henk, and P. Bruno, Phys. Rev. Lett. **89**, 086402 (2002).

[25] F. O. Schumann, C. Winkler, and J. Kirschner, Phys. Status Solidi B **246**, 1483 (2009).

[26] J. Berakdar, H. Gollisch, and R. Feder, Solid State Commun. **112**, 587 (1999).

[27] F. O. Schumann, C. Winkler, and J. Kirschner, Phys. Rev. Lett. **98**, 257604 (2007).

[28] F. O. Schumann, C. Winkler, J. Kirschner, F. Giebels, H. Gollisch, and R. Feder, Phys. Rev. Lett. **104**, 087602 (2010).

[29] R. Feder, H. Gollisch, D. Meinert, T. Scheunemann, O. M. Artamonov, S. N. Samarin, and J. Kirschner, Phys. Rev. B **58**, 16418 (1998).

[30] H. Gollisch, X. Yi, T. Scheunemann, and R. Feder, J. Phys.: Condens. Matter **11**, 9555 (1999).

[31] H. Gollisch, N. v. Schwartzenberg, and R. Feder, Phys. Rev. B **74**, 075407 (2006).

[32] F. O. Schumann, R. S. Dhaka, G. A. van Riessen, Z. Wei, and J. Kirschner, Phys. Rev. B **84**, 125106 (2011).

[33] F. Giebels, H. Gollisch, and R. Feder, J. Phys.: Condens. Matter **21**, 355002 (2009).

[34] D. B. Jochym and S. J. Clark, Phys. Rev. B **76**, 075411 (2007).

[35] G. A. van Riessen, F. O. Schumann, M. Birke, C. Winkler, and J. Kirschner, J. Phys.: Condens. Matter **20**, 442001 (2008).

[36] G. A. van Riessen, Z. Wei, R. S. Dhaka, C. Winkler, F. O. Schumann, and J. Kirschner, J. Phys.: Condens. Matter **22**, 092201 (2010).

[37] N. Mårtensson, P. Baltzer, A. Brambilla, P. A. Brühwiler, J. O. Forsell, A. Nilsson, A. Stenborg, and B. Wannberg, J. Electron Spectrosc. Relat. Phenom. **70**, 117 (1994).

[38] Kimball Physics Model ELG-2.

[39] G. A. Sawatzky, Auger photoelectron coincidence spectroscopy, in *Auger Electron Spectroscopy*, edited by C. L. Bryant and R. P. Messmer (Academic Press, San Diego, 1988).

[40] E. Jensen, R. A. Bartynski, S. L. Hulbert, and E. Johnson, Rev. Sci. Instrum. **63**, 3013 (1992).

[41] S. D. Kevan, Phys. Rev. B **28**, 2268 (1983).

[42] The theoretical band structure data required to make these plots where supplied to us by F. Giebels, H. Gollisch, and R. Feder. Details of the approach can be found under www.flapw.de.

[43] G. Ertl and J. Küppers, *Low Energy Electrons and Surface Chemistry* (VCH Verlag, Weinheim, 1985).

[44] D. P. Pappas, K. P. Kämper, B. P. Miller, H. Hopster, D. E. Fowler, C. R. Brundle, A. C. Luntz, and Z. X. Shen, Phys. Rev. Lett. **66**, 504 (1991).

[45] F. Passek, M. Donath, and K. Ertl, J. Magn. Magn. Mater. **159**, 103 (1996).

[46] M. Getzlaff, J. Bansmann, and G. Schönhense, Solid State Commun. **87**, 467 (1993).

[47] U. Rücker, H. Gollisch, and R. Feder, Phys. Rev. B **72**, 214424 (2005).

[48] S. Andersson, Surf. Sci. **18**, 325 (1969).

[49] J. Pendry, *Low Energy Electron Diffraction* (Academic Press, London, New York, 1974).

[50] J. Berakdar, S. N. Samarin, R. Herrmann, and J. Kirschner, Phys. Rev. Lett. **81**, 3535 (1998).

[51] S. Samarin, J. Berakdar, O. M. Artamonov, H. Schwabe, and J. Kirschner, Surf. Sci. **470**, 141 (2000).

[52] S. G. Louie, P. Thiry, R. Pinchaux, Y. Petroff, D. Chandesris, and J. Lecante, Phys. Rev. Lett. **44**, 549 (1980).

[53] S. D. Kevan, N. G. Stoffel, and N. V. Smith, Phys. Rev. B **31**, 1788 (1985).

[54] T. C. Hsieh, P. John, T. Miller, and T.-C. Chiang, Phys. Rev. B **35**, 3728 (1987).

[55] S. Andersson, I. Marklund, and J. Martinson, Surf. Sci. **12**, 269 (1968).

[56] S. A. Lindgren, L. Walldén, J. Rundgren, and P. Westrin, Phys. Rev. B **29**, 576 (1984).

[57] H. Gollisch and R. Feder (private communication).